

## GRAVITATIONAL MICROLENSING EVENTS FROM THE FIRST YEAR OF THE NORTHERN GALACTIC PLANE SURVEY BY THE ZWICKY TRANSIENT FACILITY

Przemek Mróz,<sup>1</sup> R. A. Street,<sup>2</sup> E. Bachelet,<sup>2</sup> E. O. Ofek,<sup>3</sup> E. C. Bellm,<sup>4</sup> R. Dekany,<sup>5</sup> D. A. Duev,<sup>1</sup> A. Gal-Yam,<sup>3</sup> M. J. Graham,<sup>1</sup> F. J. Masci,<sup>6</sup> M. Porter,<sup>5</sup> B. Rusholme,<sup>6</sup> R. M. Smith,<sup>5</sup> M. T. Soumagnac,<sup>7,3</sup> and J. Zolkower<sup>5</sup>

<sup>1</sup>*Division of Physics, Mathematics, and Astronomy, California Institute of Technology, Pasadena, CA 91125, USA*

<sup>2</sup>*Las Cumbres Observatory Global Telescope Network, 6740 Cortona Drive, Suite 102, Goleta, CA 93117, USA*

<sup>3</sup>*Department of Particle Physics and Astrophysics, Weizmann Institute of Science, 234 Herzl Street, 76100 Rehovot, Israel*

<sup>4</sup>*DIRAC Institute, Department of Astronomy, University of Washington, 3910 15th Avenue NE, Seattle, WA 98195, USA*

<sup>5</sup>*Caltech Optical Observatories, California Institute of Technology, Pasadena, CA 91125, USA*

<sup>6</sup>*IPAC, California Institute of Technology, 1200 E. California Blvd, Pasadena, CA 91125, USA*

<sup>7</sup>*Lawrence Berkeley National Laboratory, 1 Cyclotron Road, Berkeley, CA 94720, USA*

*Keywords:* gravitational lensing: micro

The Zwicky Transient Facility (ZTF) (Bellm et al. 2019; Graham et al. 2019; Masci et al. 2019) is currently surveying the entire northern sky, including dense Galactic plane fields. Here, we present preliminary results of the search for gravitational microlensing events in the ZTF data collected from the beginning of the survey (March 20, 2018) through June 30, 2019.

Searches for gravitational microlensing events have been traditionally confined to the Galactic bulge, where the probability of microlensing (and the event rate) is the highest. However, in recent years a number of bright events were discovered outside the Galactic bulge. For example, Nucita et al. (2018) found a super-Earth-mass planet in a high-magnification event TCP J05074264+2447555 detected toward the Galactic anticenter ( $l \approx 179^\circ$ ). This was the first event with the two images generated by gravitational microlensing resolved with the interferometric observations (Dong et al. 2019). Wyrzykowski et al. (2019) was able to measure all orbital parameters of the binary lens in the spectacular event Gaia16aye ( $l \approx 65^\circ$ ).

Gravitational microlensing enables one to find all types of “dark objects”, including neutron stars, single and binary black holes. While photometric observations alone are usually insufficient to determine masses of lensing objects, the combination of ground-based photometry and precise astrometric *Gaia* satellite observations will enable achieving that goal (e.g., Lu et al. 2016). Microlensing events located in the Galactic disk have, on average, larger angular Einstein radii than Galactic bulge events (Sajadian & Poleski 2019), so the astrometric signal is stronger. *Gaia* performance in the dense Galactic bulge fields is suboptimal so it is important to identify as many microlensing events as possible in the less crowded Galactic disk fields.

ZTF conducts the Galactic Plane Survey with nightly observations of all visible fields in the region  $|b| < 7^\circ$ ,  $\delta > -31^\circ$  in *g* and *r* bands. Additionally, Galactic plane fields are observed as part of ZTF collaboration and Caltech surveys.

We plan to carry out a comprehensive analysis of microlensing events in the ZTF footprint (including the measurements of the microlensing optical depth and event rate) in the future. Here, we present the first discoveries based on the first  $\sim 15$  months of the survey that demonstrate that the current observing strategy enables the identification and characterization of microlensing events in the Galactic disk fields.

Our methodology is similar to that used in our previous works (Mróz et al. 2017, 2019). We analyzed *r*-band light curves of objects associated with ZTF alerts in 408 fields at low Galactic latitudes ( $|b| \leq 20^\circ$ ); we required at least five alert detections (meaning that the object was detected on a difference image produced by the Zackay et al. (2016) algorithm). Then, we searched for objects with at least three consecutive data points that are at least  $3\sigma_{\text{base}}$  brighter than the baseline flux  $F_{\text{base}}$ , where  $F_{\text{base}}$  and  $\sigma_{\text{base}}$  were calculated using data points outside a 160 day window centered

on the event. We also fitted the microlensing point-source point-lens model to the light curves of all candidate objects. We selected candidate events that 1) do not exhibit any variability outside the window centered on the event, and 2) can be well-described by a microlensing point-lens point-source model. The light curves of selected candidates were additionally visually vetted by a human expert. The final models are based on simultaneous modeling of  $g$ - and  $r$ -band light curves.

We found 30 likely events which are listed in Table 1 and shown in Figure 1. The best-fitting model parameters are presented in Table 2. Although the current sample is relatively small, the properties of detected events are different from those of Galactic bulge events. All detected events have relatively long Einstein timescales ( $30 \lesssim t_E \lesssim 200$  d) whereas typical timescales of bulge events are shorter ( $t_E \sim 20$  d) (e.g., Mróz et al. 2017). This may be partly explained by selection biases, but we have demonstrated (Mróz et al. 2019) that nightly observations are sufficient to detect events with timescales as short as a few days. From the theoretical point of view (e.g., Sajadian & Poleski 2019), it is expected that, on average, Galactic plane events should be longer than those in the bulge direction because the source and the lens, both in the Galactic disk, are moving in a similar direction.

For four of the detected events, we were able to measure microlens parallax. ZTF18abaqxrt is particularly interesting because the source is bright ( $r \approx 14.7$ ) and so the *Gaia* satellite have likely measured the astrometric microlensing signal. We also detected five likely binary microlensing events (ZTF18ablruzq, ZTF18abqawpf, ZTF18abqazwf, ZTF18acskgwu, ZTF19aatudnj). Preliminary models indicate that these events were caused by stellar binaries.

We thank Jan Skowron for providing software for computation of microlensing magnifications. Based on observations obtained with the Samuel Oschin Telescope 48-inch and the 60-inch Telescope at the Palomar Observatory as part of the Zwicky Transient Facility project. ZTF is supported by the National Science Foundation under Grant No. AST-1440341 and a collaboration including Caltech, IPAC, the Weizmann Institute for Science, the Oskar Klein Center at Stockholm University, the University of Maryland, the University of Washington, Deutsches Elektronen-Synchrotron and Humboldt University, Los Alamos National Laboratories, the TANGO Consortium of Taiwan, the University of Wisconsin at Milwaukee, and Lawrence Berkeley National Laboratories. Operations are conducted by COO, IPAC, and UW.

**Table 1.** Gravitational microlensing events in the ZTF DR2 data

Event	R.A.	Decl.	$l$	$b$	Remarks
ZTF18aatnfd	286.633211	32.248996	63.592037	11.173057	
ZTF18aazdbym	290.784286	7.810517	43.509003	-3.416870	
ZTF18aaztjyd	326.173116	59.377872	101.101575	4.669597	
ZTF18aazwhtw	339.955528	51.647223	103.116644	-6.088552	
ZTF18abaqxrt	290.617225	1.706486	38.010990	-6.113752	
ZTF18abhxjmj	284.029167	13.152260	45.192580	4.937164	
ZTF18ablrbkj	271.850400	-10.314477	18.695441	4.908538	
ZTF18ablrdcc	271.439120	-12.014556	17.006029	4.441709	Gaia18chq
ZTF18abrluzq	284.338291	11.433438	43.790788	3.892060	binary
ZTF18abmoxlq	285.984027	-13.929477	21.832965	-9.024192	
ZTF18abnbmsr	307.149376	22.830478	64.600302	-9.235573	Gaia18cmk
ZTF18abqawpf	287.113964	1.531903	36.239259	-3.084660	binary
ZTF18abqazwf <sup>a</sup>	285.134471	30.511120	61.434070	11.599466	binary?
ZTF18abqbeqv	279.578723	7.837854	38.448164	6.467501	
ZTF18absrqlr	307.149376	22.830478	64.600302	-9.235573	
ZTF18abtnvsg	291.019150	20.478976	54.790638	2.361105	
ZTF18acskgwu	76.632447	8.425664	192.546959	-18.799234	binary
ZTF19aabbuqn	48.694244	62.343390	138.738918	3.955177	
ZTF19aaekacq	279.404621	11.200516	41.407932	8.116296	
ZTF19aainwvb	55.197569	57.955805	143.884446	2.147052	Gaia19bjq
ZTF19aamlgyh	289.114418	26.653532	59.467936	6.770307	Gaia19asx
ZTF19aamrjmu	280.734529	32.873054	62.121495	15.974788	
ZTF19aaonska	273.900566	-2.256985	26.802123	6.922664	Gaia19awc
ZTF19aaprbng	274.913476	0.590991	29.819420	7.338351	
ZTF19aatudnj <sup>a</sup>	290.663294	19.550373	53.813242	2.218551	Gaia19bzf, binary?
ZTF19aatwaux	258.208411	-27.182057	357.476262	7.002211	
ZTF19aavisrq	297.706148	34.637344	70.054958	4.102724	Gaia19dae
ZTF19aavndrc	281.836951	-4.338099	28.604991	-1.068892	
ZTF19aavnqrqt	309.034132	32.720880	73.669581	-4.807238	
ZTF19aaxsdqz	283.497170	-1.152267	32.197043	-1.092856	

<sup>a</sup>Possible microlensing event.

NOTE—Equatorial coordinates are given for the epoch J2000.

**Table 2.** Best-fitting parameters of point-lens point-source events

Event	$t_{0,\text{par}}$	$t_0$	$t_E$	$u_0$	$\pi_{E,N}$	$\pi_{E,E}$	$r_s$	$f_s$	$\chi^2/\text{dof}$
	(HJD')	(HJD')	(d)				(mag)		
ZTF18aatnfd	8254	8257.86 $^{+0.32}_{-0.30}$	76.30 $^{+7.31}_{-6.69}$	0.128 $^{+0.017}_{-0.015}$			21.81 $^{+0.14}_{-0.15}$	0.11 $^{+0.02}_{-0.01}$	3388.9/1788
ZTF18aazdbym	8273	8273.77 $^{+0.28}_{-0.28}$	32.16 $^{+4.54}_{-4.25}$	0.273 $^{+0.068}_{-0.050}$			19.01 $^{+0.26}_{-0.31}$	0.26 $^{+0.08}_{-0.06}$	494.8/492
ZTF18aaztjyd	8290	8290.11 $^{+0.19}_{-0.20}$	68.85 $^{+7.84}_{-6.74}$	0.132 $^{+0.019}_{-0.017}$			21.04 $^{+0.16}_{-0.16}$	0.78 $^{+0.12}_{-0.10}$	405.4/361
ZTF18aazwhtw	8235	8238.84 $^{+0.46}_{-0.49}$	63.04 $^{+7.16}_{-5.78}$	0.228 $^{+0.037}_{-0.033}$			20.44 $^{+0.20}_{-0.19}$	1.51 $^{+0.27}_{-0.23}$	589.0/318
ZTF18abaqxrt	8301	8301.93 $^{+0.21}_{-0.20}$	30.32 $^{+2.11}_{-1.32}$	0.673 $^{+0.050}_{-0.068}$			14.51 $^{+0.19}_{-0.14}$	0.84 $^{+0.11}_{-0.14}$	683.1/387
ZTF18abaqxrt	8301	8302.75 $^{+0.24}_{-0.23}$	33.91 $^{+4.15}_{-3.35}$	-0.581 $^{+0.096}_{-0.103}$	-0.83 $^{+0.15}_{-0.15}$	-0.00 $^{+0.28}_{-0.28}$	14.78 $^{+0.30}_{-0.30}$	0.65 $^{+0.20}_{-0.16}$	645.5/385
ZTF18abaqxrt	8301	8302.86 $^{+0.28}_{-0.28}$	33.26 $^{+4.40}_{-2.98}$	0.608 $^{+0.089}_{-0.092}$	-1.42 $^{+0.25}_{-0.29}$	-0.30 $^{+0.27}_{-0.23}$	14.69 $^{+0.28}_{-0.25}$	0.71 $^{+0.18}_{-0.16}$	645.3/385
ZTF18abhxjmj	8249	8249.14 $^{+0.21}_{-0.21}$	46.04 $^{+2.58}_{-2.35}$	0.183 $^{+0.016}_{-0.015}$			19.68 $^{+0.10}_{-0.10}$	1.06 $^{+0.10}_{-0.09}$	539.2/450
ZTF18abhxjmj	8249	8250.50 $^{+0.23}_{-0.22}$	75.08 $^{+11.64}_{-8.82}$	0.088 $^{+0.016}_{-0.014}$	0.16 $^{+0.11}_{-0.47}$	-0.72 $^{+0.21}_{-0.09}$	20.53 $^{+0.19}_{-0.19}$	0.49 $^{+0.09}_{-0.08}$	450.9/448
ZTF18abhxjmj	8249	8250.65 $^{+0.23}_{-0.24}$	79.85 $^{+11.05}_{-8.68}$	-0.087 $^{+0.013}_{-0.014}$	0.12 $^{+0.09}_{-0.30}$	-0.71 $^{+0.15}_{-0.09}$	20.54 $^{+0.18}_{-0.17}$	0.48 $^{+0.08}_{-0.07}$	451.8/448
ZTF18ablrbkj	8261	8260.87 $^{+0.99}_{-1.13}$	171.57 $^{+228.23}_{-74.59}$	0.077 $^{+0.074}_{-0.047}$			22.43 $^{+1.04}_{-0.79}$	0.24 $^{+0.26}_{-0.15}$	189.0/176
ZTF18ablrdcc	8353	8353.71 $^{+0.39}_{-0.42}$	47.76 $^{+4.93}_{-4.06}$	0.190 $^{+0.028}_{-0.028}$			19.96 $^{+0.17}_{-0.15}$	1.25 $^{+0.19}_{-0.18}$	278.3/266
ZTF18abmoxlq	8323	8323.08 $^{+0.32}_{-0.30}$	51.40 $^{+4.65}_{-2.49}$	0.448 $^{+0.033}_{-0.052}$			17.81 $^{+0.20}_{-0.12}$	0.89 $^{+0.10}_{-0.15}$	489.4/598
ZTF18abnbmsr	8363	8363.10 $^{+0.19}_{-0.18}$	38.20 $^{+3.07}_{-2.89}$	0.302 $^{+0.039}_{-0.032}$			18.97 $^{+0.15}_{-0.17}$	0.59 $^{+0.10}_{-0.08}$	707.6/537
ZTF18abqb eqv	8383	8382.46 $^{+0.89}_{-0.89}$	148.18 $^{+61.34}_{-40.00}$	0.220 $^{+0.099}_{-0.070}$	-0.28 $^{+0.08}_{-0.11}$	-0.04 $^{+0.01}_{-0.02}$	19.49 $^{+0.46}_{-0.49}$	0.07 $^{+0.04}_{-0.03}$	573.0/558
ZTF18abqb eqv	8383	8382.62 $^{+2.18}_{-2.03}$	174.92 $^{+87.56}_{-50.89}$	-0.301 $^{+0.114}_{-0.179}$	-0.17 $^{+0.06}_{-0.07}$	-0.04 $^{+0.02}_{-0.02}$	19.04 $^{+0.61}_{-0.69}$	0.11 $^{+0.10}_{-0.05}$	577.3/558
ZTF18abqb eqv	8383	8383.42 $^{+1.47}_{-1.39}$	202.51 $^{+251.02}_{-72.24}$	0.176 $^{+0.133}_{-0.105}$			19.81 $^{+1.06}_{-0.74}$	0.05 $^{+0.05}_{-0.03}$	611.2/560
ZTF18absrqlr	8363	8362.87 $^{+0.16}_{-0.16}$	37.53 $^{+2.89}_{-2.77}$	0.310 $^{+0.039}_{-0.032}$			18.93 $^{+0.15}_{-0.17}$	0.60 $^{+0.10}_{-0.08}$	648.2/490
ZTF18abtnvsg	8220	8219.98 $^{+0.27}_{-0.32}$	108.56 $^{+38.17}_{-23.98}$	0.046 $^{+0.017}_{-0.014}$			21.93 $^{+0.39}_{-0.35}$	0.09 $^{+0.03}_{-0.03}$	430.5/287
ZTF19aabbuqn	8506	8506.14 $^{+0.42}_{-0.41}$	25.80 $^{+5.29}_{-3.99}$	0.478 $^{+0.139}_{-0.121}$			19.03 $^{+0.45}_{-0.44}$	0.54 $^{+0.27}_{-0.18}$	763.0/296
ZTF19aaekacq	8544	8544.72 $^{+0.54}_{-0.52}$	79.53 $^{+10.20}_{-9.20}$	0.224 $^{+0.076}_{-0.060}$			18.65 $^{+0.26}_{-0.28}$	0.21 $^{+0.06}_{-0.04}$	465.4/546
ZTF19aainwvb	8656	8615.99 $^{+0.59}_{-0.60}$	137.66 $^{+6.89}_{-5.42}$	-0.098 $^{+0.029}_{-0.022}$	-0.25 $^{+0.01}_{-0.01}$	0.24 $^{+0.02}_{-0.02}$	18.48 $^{+0.09}_{-0.06}$	0.99 $^{+0.06}_{-0.08}$	1028.2/554
ZTF19aainwvb	8656	8651.56 $^{+0.44}_{-0.45}$	134.57 $^{+2.67}_{-2.49}$	0.349 $^{+0.009}_{-0.009}$			18.21 $^{+0.04}_{-0.04}$	1.34 $^{+0.05}_{-0.04}$	2294.7/558
ZTF19aamlg yh	8567	8567.08 $^{+0.16}_{-0.16}$	33.43 $^{+2.90}_{-2.43}$	0.149 $^{+0.018}_{-0.017}$			19.04 $^{+0.14}_{-0.13}$	0.84 $^{+0.11}_{-0.10}$	937.4/652
ZTF19aamrjmu	8579	8579.78 $^{+0.11}_{-0.11}$	60.30 $^{+3.24}_{-3.00}$	0.148 $^{+0.011}_{-0.011}$			20.10 $^{+0.09}_{-0.08}$	0.78 $^{+0.06}_{-0.06}$	1875.8/1203
ZTF19aaonska	8613	8613.12 $^{+0.34}_{-0.32}$	70.20 $^{+4.24}_{-3.83}$	0.280 $^{+0.025}_{-0.025}$			19.10 $^{+0.12}_{-0.11}$	0.89 $^{+0.09}_{-0.09}$	603.6/404
ZTF19aprbng	8629	8630.34 $^{+1.25}_{-1.22}$	112.61 $^{+31.69}_{-17.91}$	0.593 $^{+0.163}_{-0.170}$			19.13 $^{+0.56}_{-0.45}$	0.57 $^{+0.30}_{-0.23}$	515.6/469
ZTF19aatwaux	8636	8636.95 $^{+0.52}_{-0.52}$	53.34 $^{+8.14}_{-5.64}$	0.162 $^{+0.040}_{-0.039}$			19.28 $^{+0.26}_{-0.22}$	0.79 $^{+0.18}_{-0.17}$	342.9/380
ZTF19aavisrq	8651	8651.79 $^{+0.02}_{-0.02}$	96.39 $^{+6.61}_{-5.83}$	0.017 $^{+0.001}_{-0.001}$			20.58 $^{+0.08}_{-0.07}$	0.14 $^{+0.01}_{-0.01}$	564.3/595
ZTF19aavndrc	8637	8637.42 $^{+0.15}_{-0.16}$	73.95 $^{+4.39}_{-3.91}$	0.095 $^{+0.008}_{-0.008}$			19.90 $^{+0.09}_{-0.09}$	0.39 $^{+0.03}_{-0.03}$	429.2/458
ZTF19aavn rqt	8721	8721.03 $^{+0.53}_{-0.49}$	77.21 $^{+4.10}_{-2.25}$	0.631 $^{+0.027}_{-0.048}$			17.17 $^{+0.14}_{-0.08}$	0.92 $^{+0.07}_{-0.11}$	1651.8/673
ZTF19aaxsdqz	8676	8676.54 $^{+0.14}_{-0.14}$	62.54 $^{+3.75}_{-2.90}$	0.180 $^{+0.013}_{-0.014}$			18.99 $^{+0.10}_{-0.08}$	1.01 $^{+0.08}_{-0.09}$	331.2/282

NOTE—HJD'=HJD-2450000. Microlensing point-source point-lens models have the following parameters:  $t_0$  and  $u_0$  – time and separation during the closest approach between the lens and the source,  $t_E$  – Einstein timescale,  $\pi_{E,N}$  and  $\pi_{E,E}$  – North and East components of the microlensing parallax vector,  $r_s$  –  $r$ -band brightness of the source,  $f_s$  – blending parameter.  $t_{0,\text{par}}$  defines the coordinate system for parallax measurements and is not a fit parameter.

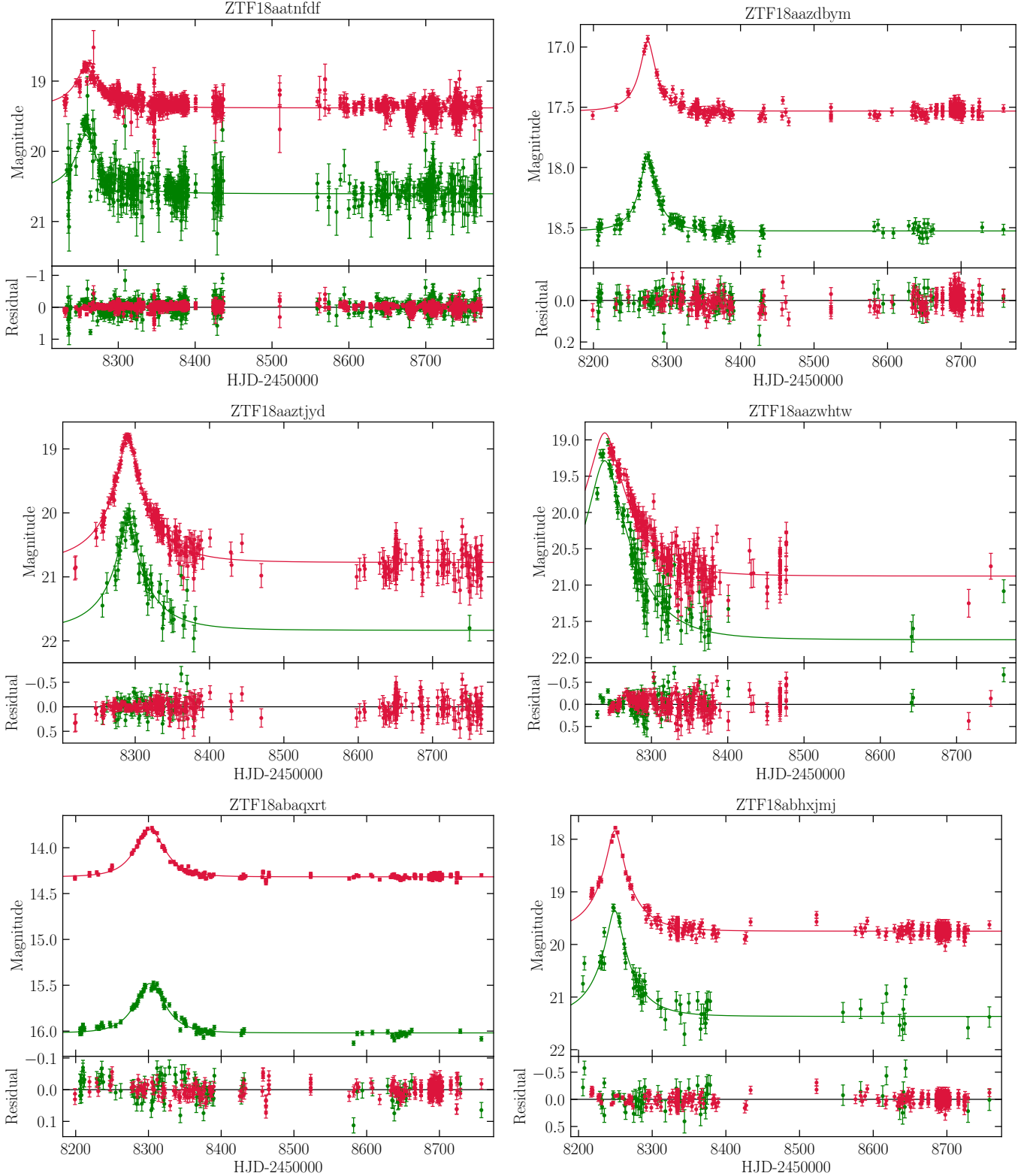


**Figure 1.** Light curves of detected microlensing events. Green and red points were taken in  $g$  and  $r$  filters, respectively.

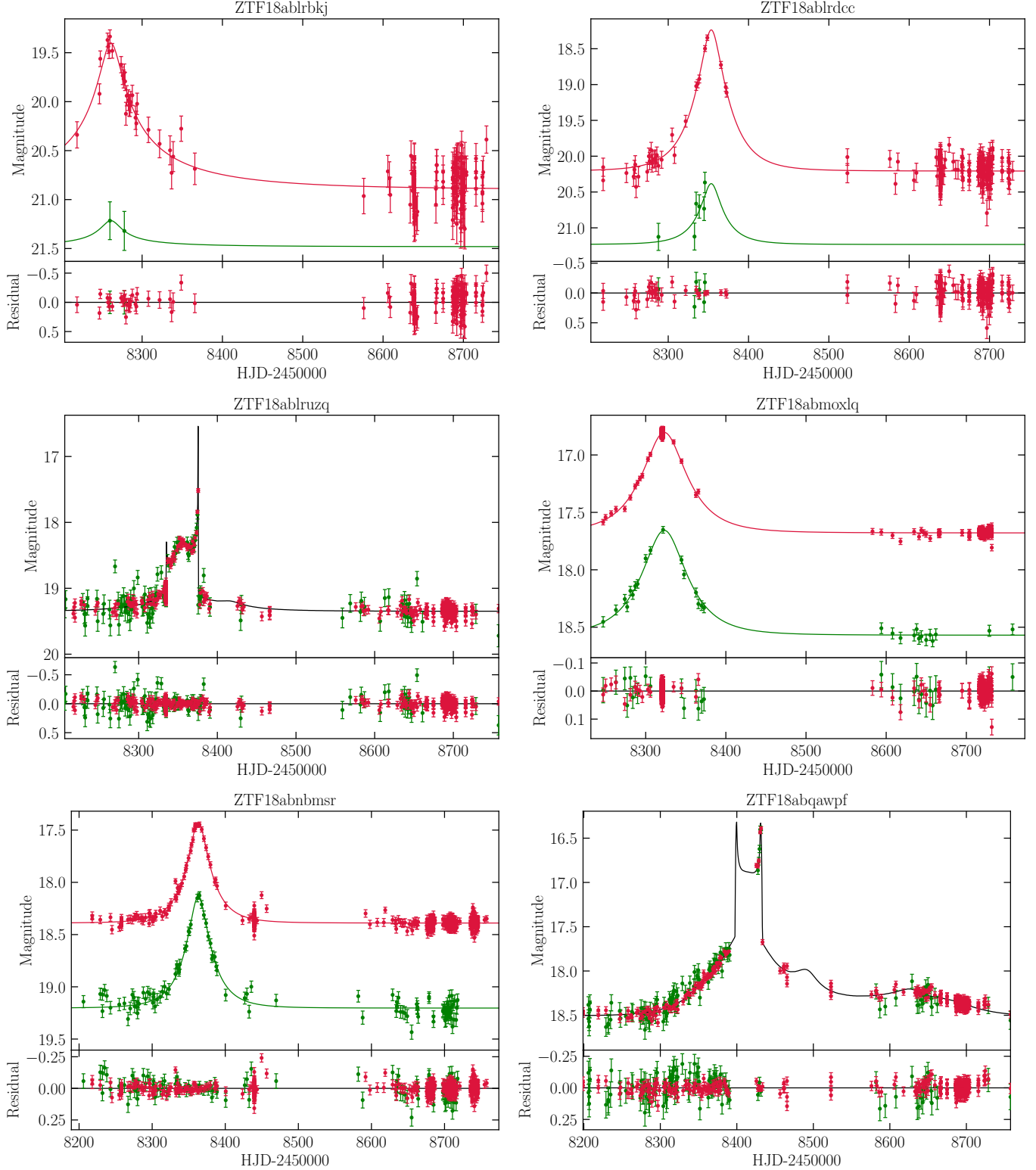


**Figure 1.** Light curves of detected microlensing events. Green and red points were taken in *g* and *r* filters, respectively.

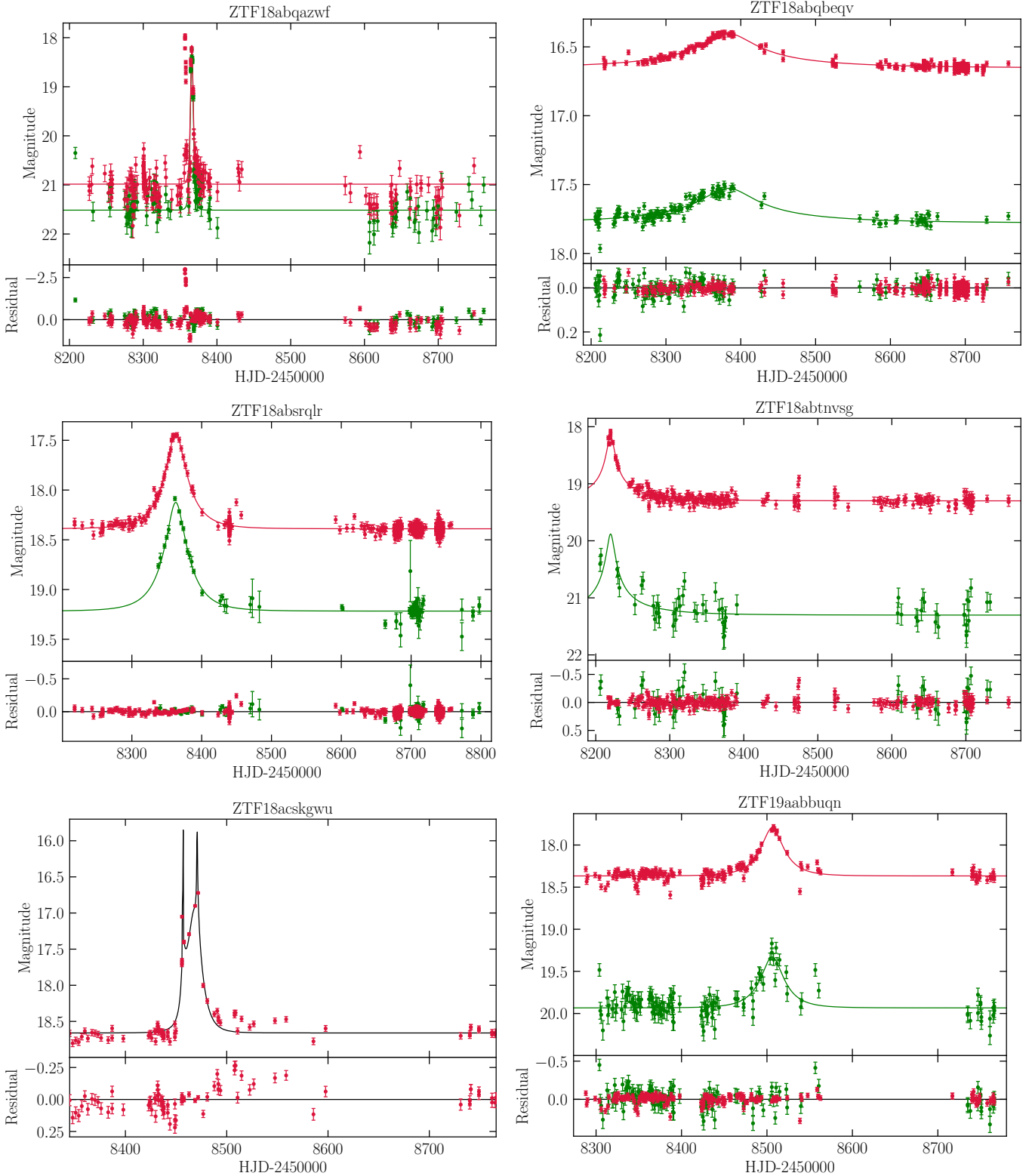


**Figure 1.** Light curves of detected microlensing events. Green and red points were taken in *g* and *r* filters, respectively.

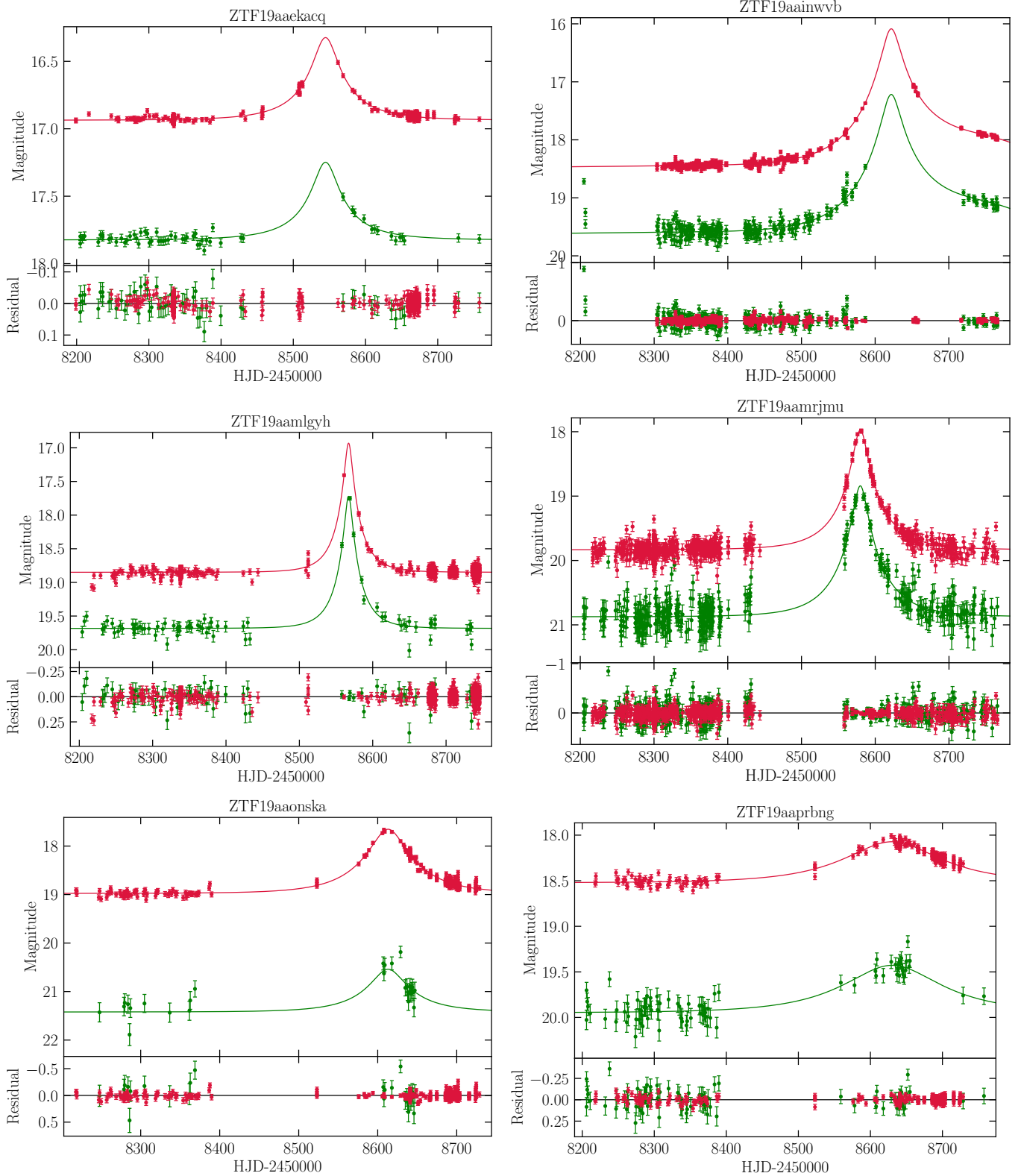


**Figure 1.** Light curves of detected microlensing events. Green and red points were taken in *g* and *r* filters, respectively.

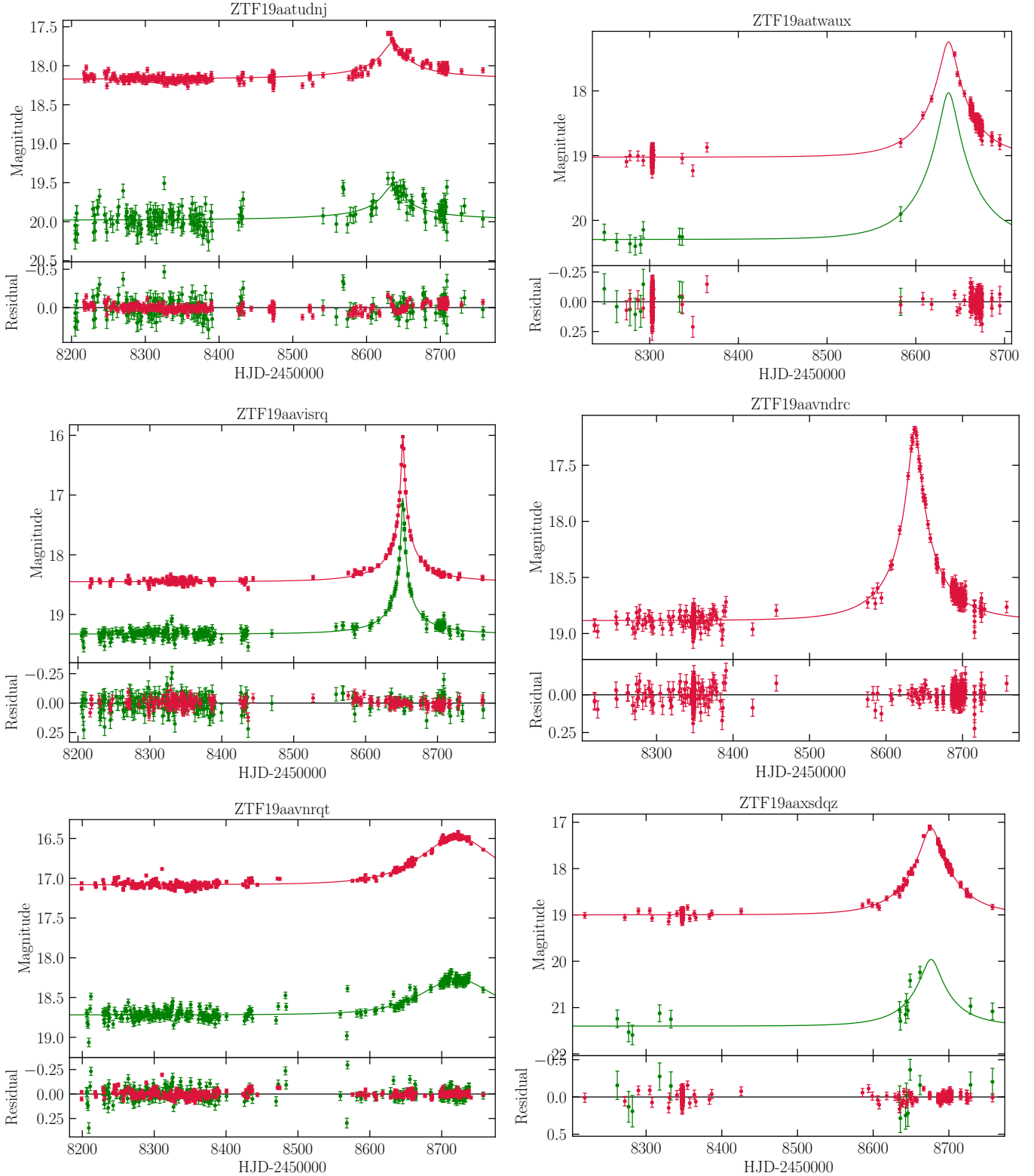


**Figure 1.** Light curves of detected microlensing events. Green and red points were taken in *g* and *r* filters, respectively.

## REFERENCES

- Bellm, E. C., Kulkarni, S. R., Graham, M. J., et al. 2019, *PASP*, 131, 018002
- Dong, S., Mérand, A., Delplancke-Ströbele, F., et al. 2019, *ApJ*, 871, 70
- Graham, M. J., Kulkarni, S. R., Bellm, E. C., et al. 2019, *PASP*, 131, 078001
- Lu, J. R., Sinukoff, E., Ofek, E. O., et al. 2016, *ApJ*, 830, 41
- Masci, F. J., Laher, R. R., Rusholme, B., et al. 2019, *PASP*, 131, 018003
- Mróz, P., Udalski, A., Skowron, J., et al. 2017, *Nature*, 548, 183
- Mróz, P., Udalski, A., Skowron, J., et al. 2019, *ApJS*, 244, 29
- Nucita, A. A., Licchelli, D., De Paolis, F., et al. 2018, *MNRAS*, 476, 2962
- Sajadian, S., & Poleski, R. 2019, *ApJ*, 871, 205
- Wyrzykowski, L., Mróz, P., Rybicki, K. A., et al. 2019, arXiv e-prints, arXiv:1901.07281
- Zackay, B., Ofek, E. O., Gal-Yam, A. 2016, *ApJ*, 830, 27